

DFSZ Axion Dark Matter Search around 4.55 μeV

Andrew K. Yi,^{1,2} Saebyeok Ahn,^{1,2} Çağlar Kutlu,^{1,2} JinMyeong Kim,^{1,2} Byeong Rok Ko,^{2,*} Boris I. Ivanov,² HeeSu Byun,² Arjan F. van Loo,^{3,4} SeongTae Park,² Junu Jeong,² Ohjoon Kwon,² Yasunobu Nakamura,^{3,4} Sergey V. Uchaikin,² Jihoon Choi,^{2,†} Soohyung Lee,² MyeongJae Lee,^{2,‡} Yun Chang Shin,² Jinsu Kim,^{1,2} Doyu Lee,^{2,§} Danho Ahn,^{1,2} SungJae Bae,^{1,2} Jiwon Lee,^{1,2} Younggeun Kim,² Violeta Gkika,² Ki Woong Lee,² Seonjeong Oh,² Taehyeon Seong,² DongMin Kim,² Woohyun Chung,² Andrei Matlashov,² SungWoo Youn,² and Yannis K. Semertzidis^{2,1}

¹*Dept. of Physics, Korea Advanced Institute of Science and Technology, Daejeon 34141, Republic of Korea*

²*Center for Axion and Precision Physics Research, Institute for Basic Science, Daejeon 34051, Republic of Korea*

³*RIKEN Center for Quantum Computing (RQC), Wako, Saitama 351-0198, Japan*

⁴*Dept. of Applied Physics, Graduate School of Engineering, The University of Tokyo, Bunkyo-ku, Tokyo 113-8656, Japan*

We report an axion dark matter search at Dine-Fischler-Srednicki-Zhitnitskii sensitivity with the CAPP-12TB haloscope, assuming axions contribute 100% of the local dark matter density. The search excluded the axion–photon coupling $g_{a\gamma\gamma}$ down to about $6.2 \times 10^{-16} \text{ GeV}^{-1}$ over the axion mass range between 4.51 and 4.59 μeV at a 90% confidence level. The achieved experimental sensitivity can also exclude Kim-Shifman-Vainshtein-Zakharov axion dark matter that makes up just 13% of the local dark matter density. The CAPP-12TB haloscope will continue the search over a wide range of axion masses.

The standard model of Big Bang cosmology combined with precision cosmological measurements strongly suggest that cold dark matter (CDM) constitutes about 85% of the matter and 27% of the energy density in the Universe [1]. CDM is a subject of beyond the standard model of particle physics (SM) and remains hidden to date. The axion [2] stems from the breakdown of a new global symmetry introduced by Peccei and Quinn [3] to solve the strong CP problem in the SM [4], and is one of the most prominent CDM candidates, provided its mass is above $\mathcal{O}(\mu\text{eV})$ according to the original work [5], or above $\mathcal{O}(\text{peV})$ by more recent works [6], and below $\mathcal{O}(\text{meV})$ [7].

The axion haloscope search proposed by Sikivie [8] exploits the axion–photon coupling $g_{a\gamma\gamma}$ in a microwave cavity permeated with a static magnetic field, which results in resonant conversions of axions to photons when the axion mass m_a matches the frequency of the cavity mode ν , $m_a = h\nu/c^2$. The two most popular models, Kim-Shifman-Vainshtein-Zakharov (KSVZ) [9] and Dine-Fischler-Srednicki-Zhitnitskii (DFSZ) [10], benchmark the axion–photon couplings with $g_\gamma = -0.97$ and 0.36, respectively, where g_γ is a dimensionless coupling constant and comes from $g_{a\gamma\gamma} = \frac{\alpha g_\gamma}{\pi f_a}$ along with the axion decay constant f_a and the fine structure constant α . The use of a high quality microwave cavity makes the axion haloscope the most promising method for axion dark matter searches in the microwave region.

In this Letter, we report a DFSZ axion dark matter search using the CAPP-12TB haloscope at the Institute for Basic Science (IBS) Center for Axion and Precision Physics Research (CAPP) [11, 12]. Here, 12TB stands for our solenoid specifications, the central magnetic field of 12 T and the Big bore of 320 mm [13]. To date, DFSZ axion dark matter sensitive searches were only achieved by the Axion Dark Matter eXperiment (ADMX) [14, 15].

The CAPP-12TB haloscope depicted in Fig. 1 comprises a 36.85 L frequency tunable copper cylindrical cavity placed at the magnet center, a superconducting solenoid whose average magnetic field B_{avg} over the cavity volume V is 10.31 T, and a heterodyne receiver chain with a Josephson Parametric Amplifier (JPA) as the first amplifier. The experiment maintained the physical temperatures of the cavity and the JPA at around 25 mK using a dilution refrigerator DRS-1000 [16] whose cooling power was measured to be about 1 mW at 90 mK without any load.

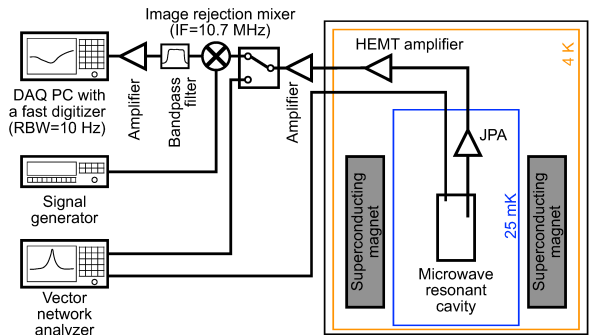


FIG. 1: Schematic of the CAPP-12TB haloscope.

The detected axion signal power is expected to be

$$\begin{aligned}
 P_a^{a\gamma\gamma} &= 22.51 \text{ yW} \left(\frac{g_\gamma}{0.36} \right)^2 \left(\frac{B_{\text{avg}}}{10.31 \text{ T}} \right)^2 \\
 &\times \left(\frac{V}{36.85 \text{ L}} \right) \left(\frac{C}{0.6} \right) \left(\frac{Q_L}{35000} \right) \\
 &\times \left(\frac{\nu}{1.1 \text{ GHz}} \right) \left(\frac{\rho_a}{0.45 \text{ GeV/cm}^3} \right) \quad (1)
 \end{aligned}$$

when the axion mass matches the frequency of the cavity mode $m_a = h\nu/c^2$ and the cavity mode coupling to the receiver, β , is 2. In Eq. (1), C is the cavity-mode-dependent form factor which in practice includes the axion-photon interaction energy normalized by the energy stored in the electric and magnetic fields over the cavity volume [17], Q_L is the loaded quality factor of the cavity mode, and ρ_a is the local dark matter density. In this work, we have assumed axions make up 100% of the local dark matter density, i.e., $\rho_a = 0.45$ GeV/cm³, to explore the axion-photon coupling. As the CAPP-12TB axion haloscope has cylindrical geometry, the chosen cavity mode for this axion dark matter search is the TM₀₁₀-like mode, to maximize C . Assuming the standard halo model of axion dark matter, the signal power given in Eq. (1) would then be distributed over a boosted Maxwellian shape with an axion rms speed of about 270 km/s, and the Earth rms speed of 230 km/s with respect to the galaxy frame [18], respectively, which is the model for this work.

We have realized a frequency tuning mechanism operating in a cryogenic and high magnetic field environment employing a piezoelectric motor manufactured by attocube [19]. The motor sits on the top end cap of the cavity and links the tuning rod directly through a crank arm, where the tuning rod is a copper cylinder whose diameter is about a tenth of the cavity diameter. By rotating the tuning rod about the tuning axle, we tuned the cavity modes over the frequency range considered in this work. Another attocube piezoelectric motor for an antenna has been adopted to adjust β that was measured to be between 1.8 and 2.2 during data taking through the “Strong” line in Fig. 2. A fixed antenna minimally coupled to the cavity has also been implemented at the end of the “Weak” line. The Q_L values of the TM₀₁₀-like modes were measured to be over 35000, and the form factors for these modes were calculated to be about 0.6 using a finite element method calculation [20, 21].

Our receiver chain consists of a single data acquisition (DAQ) channel. As shown in Fig. 2, power from the cavity goes through a directional coupler, two circulators, and a JPA, which were located in the magnetic-field cancellation region realized by a magnet system [13]. The JPA is described and characterized in detail elsewhere [22, 23], and here we describe our JPA operation scheme for this work. The JPA profiles were probed with +1 kHz offset from the JPA resonant frequencies which were set accordingly to the target frequencies, where the target frequencies are the central frequencies of each individual power spectra. The JPA gains were measured through the “Bypass” line including a 50- Ω termination, shown as the noise source in Fig. 2 by the microwave switch, with a vector network analyzer (VNA) as the power ratio with and without the pump power through the “Pump” line for the parametric amplification. We required the JPA gains at the probe tones to be 20 ± 0.4 dB

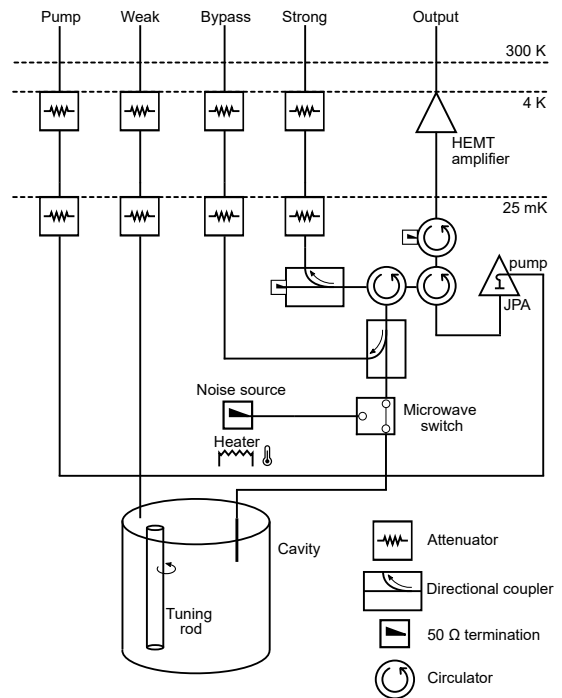


FIG. 2: CAPP-12TB receiver diagram.

and thus always obtained gains of around 20 dB at the JPA resonant frequencies. Our target frequencies had +100 kHz offset from the JPA resonant frequencies, so the JPA amplification for this axion dark matter search was about 17 dB on the cavity modes over the frequency range, while those at -100 and +100 kHz detuned from the cavity modes were about 20 and 14 dB, respectively, with JPA bandwidths of about 190 kHz. The noise temperatures of the JPA were measured at the target frequencies using the power ratio with and without JPA amplification [15]. The power was transferred from the noise source shown in Fig. 2, whose physical temperature was maintained at about 25 mK, resulting in a noise temperature of about 34 mK for the frequency range considered in this Letter. Together with the noise temperatures of the receiver chain without the JPA amplification, explained below, and the aforementioned JPA gains, it is possible to extract the added noise temperature from the JPA, which was about 60 mK. The *in-situ* JPA gains through the line including the cavity instead of the 50- Ω termination were measured using the same boundary conditions above, during data collection. The power was further amplified inside the fridge using two serial LNF-LNC0.6_2A [24] High-Electron-Mobility Transistor (HEMT) amplifiers anchored at the 4-K stage.

After further processing outside the fridge (see also Fig. 1), which comprises of downconversion to the intermediate frequency (IF) of 10.7 MHz with an image rejection mixer [25] and additional amplification, the power was then digitized and converted into a frequency spec-

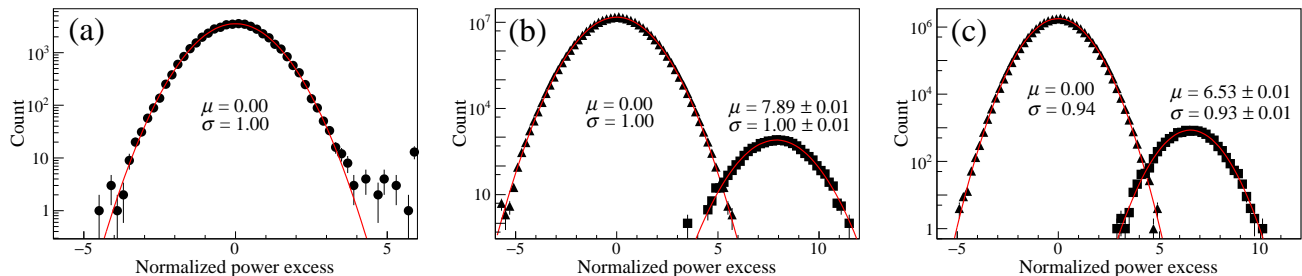


FIG. 3: Circles in (a) show the distribution of the normalized power excess from all the frequency points in the normalized grand power spectrum from the CAPP-12TB experiment, after applying a frequency-independent scale factor of 0.94. (b) shows the distributions of the normalized power excess from 10000 simulated CAPP-12TB experiments by co-adding 81 adjacent 50 Hz power spectral lines after the background subtraction using the simulation input, and (c) shows those by 9 adjacent 450 Hz power spectral lines and the χ^2 fit. Rectangles and triangles in (b) and (c) are from the frequency with the simulated axion signals and frequencies with background only, respectively. Lines are a Gaussian fit resulting in μ (mean) and σ (width).

trum over a span from -500 to $+500$ kHz with respect to the IF with a resolution bandwidth (RBW) of 10 Hz utilizing the fast DAQ system in Ref. [26], accessed via CULDAQ [27].

The gain and noise temperature from the receiver chain other than the JPA were measured using the Y-factor method [28] by varying the physical temperature of the noise source up to 400 mK without JPA amplification. Accordingly they include all the attenuation and noise from the rest of the chain and are about 104 dB and 1.2 K, respectively, where the latter contributes about 25 mK to the measured total noise temperature with the 50- Ω termination according to Ref. [29] at the target frequencies. The total gain of the receiver chain including the *in-situ* JPA gain is about 121 dB at the target frequencies.

The total system noise temperature T_n , which is a sum of the noise temperatures of the cavity and the receiver chain, was obtained by correcting for the total gain in power and parameterized with a Savitzky-Golay (SG) filter [30]. The parameters of the SG filter were a polynomial of degree 4 and a 2001-point window at an RBW of 10 Hz. In each power spectrum, the extracted total noise temperature at the cavity mode ν is about 215 mK as an approximately Lorentzian peak, which is attributed to the tuning rod being hotter than the cavity barrel due to the poor thermal link between them. The total noise temperatures at -100 and $+100$ kHz detuned from the cavity mode were typically 130 and 185 mK, which mainly comes from the JPA gain profile that determines the noise temperature profiles of the chain after the JPA [29] and of the JPA itself as well. With the cavity as a noise source, the T_n was also measured by the power ratio with and without the JPA amplification as applied in the JPA noise measurement above. The difference between the two noise measurements was 5–10% depending on the frequency, which was taken as the systematic uncertainty of our T_n .

The signal-to-noise ratio (SNR) in this work is defined by the signal power for the DFSZ axion dark matter coupling $g_{a\gamma\gamma}^{\text{DFSZ}}$

$$\text{SNR} = \frac{P_a^{\text{DFSZ}}}{P_n} \sqrt{b_a \Delta t} = \frac{P_a^{\text{DFSZ}}}{k_B b_a T_n} \sqrt{N} = \frac{P_a^{\text{DFSZ}}}{\sigma_{P_n}} \quad (2)$$

according to the radiometer equation [31], where P_n and σ_{P_n} are the total noise power and its fluctuation, respectively. b_a is the axion signal window which is about 4050 Hz for the axion masses considered in this Letter, Δt is the integration time at each step, N is the number of power spectra, and k_B is the Boltzmann constant. We acquired data from March 1st to 18th in 2022 including system maintenance. A total of 1996 resonant frequencies were scanned over a search range of 20.06 MHz with frequency steps of 10 kHz, except for 380 kHz due to the mode crossings around an axion mass of $4.527 \mu\text{eV}$. We made sure that the cavity simulation [20, 21] also observed the mode crossings. Power spectra were taken with $\Delta t \sim 500$ s at each step, which resulted in $N \sim 5000$ with our RBW choice of 10 Hz [26]. The power spectra were averaged and then processed through the analysis procedure addressed below. The achieved SNR values over the search range were generally higher than 5.

The data analysis process basically follows the axion haloscope analysis procedures developed to date [32–34]. From each power spectrum, only the axion signal sensitive region around the cavity mode was used. Furthermore, a span of 150 kHz centered at the target frequency of the cavity mode was selected to avoid the presence of the pump tone and lower JPA gain or, equivalently, higher noise contribution. The frequency span allows 15 power spectra to overlap in most of the frequency range with our frequency steps of 10 kHz.

First, narrow spikes in each power spectrum were removed with a filtering procedure similar to the one by the Haloscope At Yale Sensitive To Axion CDM [33]. Each power spectrum was parameterized by a χ^2 fit and

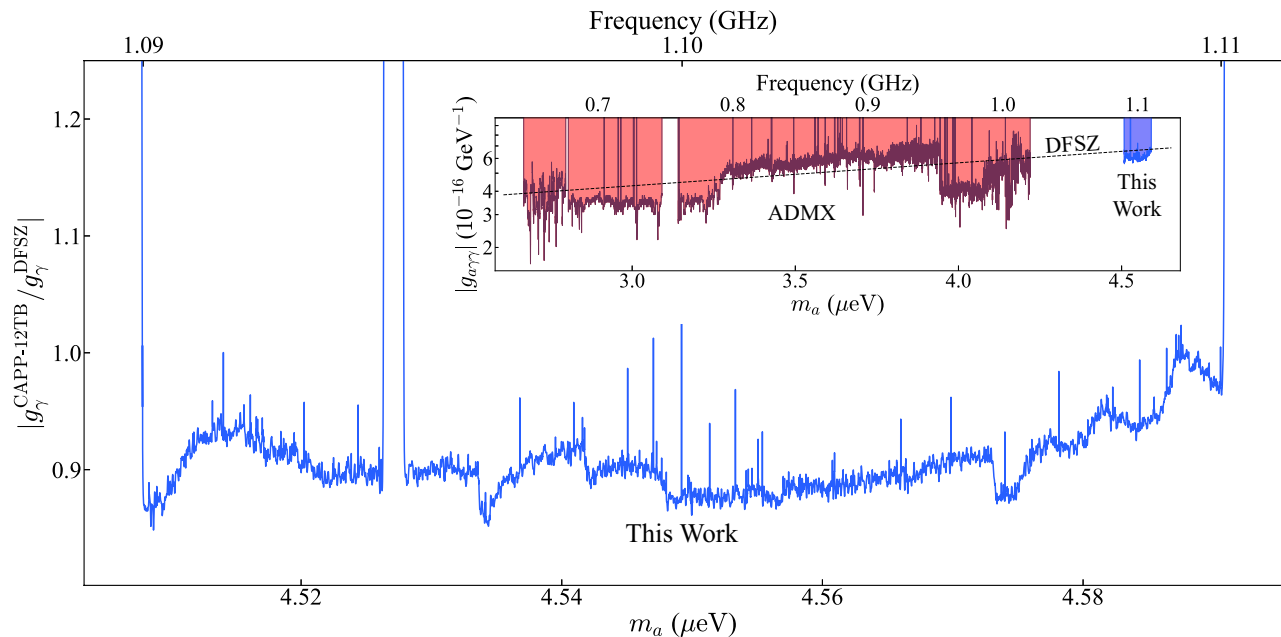


FIG. 4: Blue solid line is the excluded parameter space at a 90% confidence level by this work. Note the mode crossing around an axion mass of $4.527 \mu\text{eV}$, which is predicted by a finite element method calculation [20, 21]. The inset shows exclusion limits from other axion haloscope searches sensitive to the DFSZ axion dark matter [14, 15] as well as that from this work. The intermittent spikes resulted from the filtering procedure (see the text).

then went through the filtering at an RBW of 10 Hz. The fit function is the product of a five-parameter function [32] for the overall noise profile of the receiver chain, a Lorentzian for the JPA gain profile, and quadratic polynomial for the noise profile depending on the JPA gain profile. In the fit, the minimum of the quadratic function was constrained to be located at the JPA resonant frequency according to the JPA gain profile and the JPA gain at the target frequency was required to be consistent with the aforementioned measurement. This χ^2 parametrization improved the SNR efficiency by about 10% in the end albeit having almost the same rescanned candidates compared to that by an SG filter using the same parameters mentioned above. Five nonoverlapping frequency points in each power spectrum were merged so that the RBW became 50 Hz, we went through the filtering procedure again and applied the background subtraction. After the background subtraction, each power spectral line and its fluctuation in each spectrum were scaled by the expected total axion signal power, where the scaling across the spectrum follows the Lorentzian line shape characterized by the cavity Q_L [33]. Allowing the overlaps among the power spectra, all the power spectra were then combined to produce a single power spectrum and the associated power fluctuations were also propagated accordingly. The RBW of the combined spectrum was further reduced to 450 Hz by merging nine nonoverlapping frequency points. From the combined spectrum, our “grand power spectrum” was con-

structed by co-adding [32] nine adjacent 450 Hz power spectral lines, which retained more than 99.9% of the putative axion signal power, where each power spectral line was weighted by the axion signal shape, which follows a boosted Maxwellian [33]. The grand power spectrum was normalized by σ_{P_n} which was also weighted according to the axion signal shape [33] and co-added [32]. A frequency-independent scale factor of 0.94 was applied to remedy the bias in power excess induced from the background subtraction [34], resulting in a normalized grand power spectrum following the standard Gaussian as shown in Fig. 3(a).

With such standard Gaussian statistics, we applied a threshold of $3.718\sigma_{P_n}$ and 33 power spectral lines located in 14 individual power spectra exceeded the cut. After rescanning the 14 individual power spectra with sufficiently high statistics, no power spectral lines were found to exceed the cut.

The SNR efficiency was estimated from 10000 simulated CAPP-12TB experiments having axion signals at a particular frequency on top of the CAPP-12TB background [34]. Figures 3(b) and (c) show the normalized power excess distributions from the simulation, where Fig. 3(b) was obtained by co-adding 81 adjacent 50 Hz power spectral lines after the background subtraction using the simulation input, and Fig. 3(c) by 9 adjacent 450 Hz power spectral lines and our χ^2 fit. The narrow width of the normalized power excess distribution 0.94 induced from the background subtraction shown in the

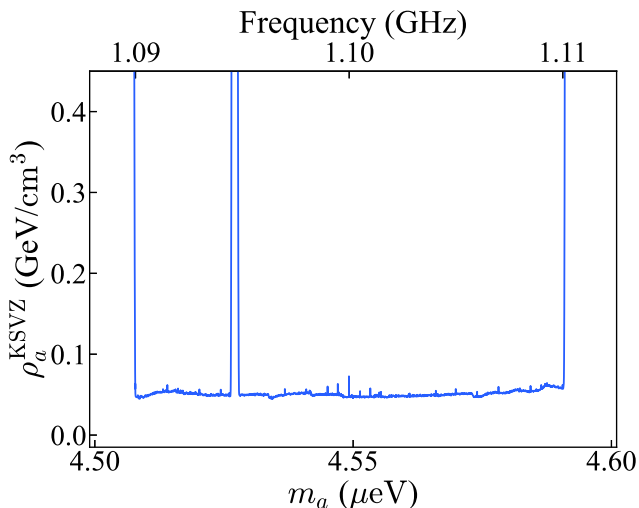


FIG. 5: Exclusion limits for the KSVZ axion dark matter density ρ_a^{KSVZ} at a 90% confidence level.

CAPP-12TB data was also demonstrated by the large statistics simulation data, as shown in the solid triangles in Fig. 3(c). From the distributions in Figs. 3(b) and (c), our SNR efficiency is estimated to be 88%, which can be mainly attributed to the background subtraction. Note that the signal weighting in the co-adding procedure can degrade the SNR depending on the RBW, and our SNR efficiency includes a degradation of about 5% due to the RBW reduction from 50 to 450 Hz [35]. Other SNR inefficiencies, from the filtering for the individual power spectrum and the axion signal misalignment with respect to the RBW of 450 Hz, were negligible compared to that from the background subtraction [12]. The line attenuation from the cavity to the microwave switch was not considered in our gain measurement mentioned above. Using a VNA and “Strong” line, we measured two reflected powers, one from the cavity and the other from the switch. In order to obtain the fully reflected power, the switch was configured to float between the two switch ports and the cavity off-resonant frequency range was inspected. The line attenuation was measured by taking half of the difference between the two reflection measurements and was 0.3–0.5 dB depending on the frequency. The total SNR efficiency taking into account for the background subtraction, the additional line attenuation, and the systematic uncertainty was reflected in our exclusion limits.

We set the 90% upper limits of $g_{a\gamma\gamma}$ for $4.51 < m_a < 4.59 \mu\text{eV}$. Figure 4 shows the excluded parameter space at a 90% confidence level (CL) from the CAPP-12TB experiment. Using the achieved experimental sensitivity, we also excluded KSVZ axion dark matter, which makes up 13% of the local dark matter density, as shown in Fig. 5. Our results are the most sensitive in the relevant axion mass range to date.

In summary, we report a search for DFSZ axion dark matter using the CAPP-12TB haloscope. The CAPP-12TB experiment has been pushing all the experimental parameters to reach state-of-the-art performance. With such performance, the CAPP-12TB experiment has achieved axion–photon couplings $g_{a\gamma\gamma}$ of about $6.2 \times 10^{-16} \text{ GeV}^{-1}$ which is beyond the DFSZ axion dark matter coupling, over the axion mass range between 4.51 and 4.59 μeV at a 90% CL. This is an unprecedented sensitivity tier in the mass range to date. We expect that CAPP-12TB as a state-of-the-art axion haloscope will continue sensitive searches over a wide range of axion masses with high-frequency [36] and high-quality cavity designs [37].

This work was supported by IBS-R017-D1-2022-a00.

* Corresponding author : brko@ibs.re.kr

† Now at Korea Astronomy and Space Science Institute, Daejeon 34055, Republic of Korea

‡ Now at Dept. of Physics, Sungkyunkwan University, Suwon 16419, Republic of Korea

§ Now at Samsung Electronics, Gyeonggi-do 16677, Republic of Korea

- [1] P. A. R. Ade *et al.* (Planck Collaboration), *Astron. Astrophys.* **594**, A13 (2016).
- [2] S. Weinberg, *Phys. Rev. Lett.* **40**, 223 (1978); F. Wilczek, *Phys. Rev. Lett.* **40**, 279 (1978).
- [3] R. D. Peccei and H. R. Quinn, *Phys. Rev. Lett.* **38**, 1440 (1977).
- [4] G. 't Hooft, *Phys. Rev. Lett.* **37**, 8 (1976); G. 't Hooft, *Phys. Rev. D* **14**, 3432 (1976) [Erratum-*ibid.* **D 18**, 2199 (1978)]; J. H. Smith, E. M. Purcell, and N. F. Ramsey, *Phys. Rev.* **108**, 120 (1957); W. B. Dress, P. D. Miller, J. M. Pendlebury, P. Perrin, and N. F. Ramsey, *Phys. Rev. D* **15**, 9 (1977); I. S. Altarev *et al.*, *Nucl. Phys. A* **341**, 269 (1980).
- [5] J. Preskill, M. B. Wise, and F. Wilczek, *Phys. Lett. B* **120**, 127 (1983); L. F. Abbott and P. Sikivie, *Phys. Lett. B* **120**, 133 (1983); M. Dine and W. Fischler, *Phys. Lett. B* **120**, 137 (1983).
- [6] Fuminobu Takahashi, Wen Yin, and Alan H. Guth, *Phys. Rev. D* **98**, 015042 (2018); Peter W. Graham and Adam Scherlis, *Phys. Rev. D* **98**, 035017 (2018).
- [7] John Ellis and K. A. Olive, *Phys. Lett. B* **193**, 525 (1987); Georg Raffelt and David Seckel, *Phys. Rev. Lett.* **60**, 1793 (1988); Michael S. Turner, *Phys. Rev. Lett.* **60**, 1797 (1988); Hans-Thomas Janka, Wolfgang Keil, Georg Raffelt, and David Seckel, *Phys. Rev. Lett.* **76**, 2621 (1996); Wolfgang Keil *et al.*, *Phys. Rev. D* **56**, 2419 (1997).
- [8] P. Sikivie, *Phys. Rev. Lett.* **51**, 1415 (1983); *Phys. Rev. D* **32**, 2988 (1985).
- [9] J. E. Kim, *Phys. Rev. Lett.* **43**, 103 (1979); M. A. Shifman, A. I. Vainshtein, and V. I. Zakharov, *Nucl. Phys. B* **166**, 493 (1980).
- [10] A. R. Zhitnitskii, *Yad. Fiz.* **31**, 497 (1980) [*Sov. J. Nucl. Phys.* **31**, 260 (1980)]; M. Dine, W. Fischler, and M. Srednicki, *Phys. Lett. B* **140**, 199 (1981).
- [11] Yannis K. Semertzidis *et al.*, [arXiv:1910.11591](https://arxiv.org/abs/1910.11591); J. Jeong

- et al.*, Phys. Rev. Lett. **125**, 221302 (2020); O. Kwon *et al.*, Phys. Rev. Lett. **126**, 191802 (2021); Y. Lee *et al.*, Phys. Rev. Lett. **128**, 241805 (2022).
- [12] S. Lee, S. Ahn, J. Choi, B. R. Ko, and Y. K. Semertzidis, Phys. Rev. Lett. **124**, 101802 (2020).
- [13] W. Ma *et al.*, IOP Conf. Ser.: Mater. Sci. Eng. **502**, 012104 (2019).
- [14] N. Du *et al.* (ADMX Collaboration), Phys. Rev. Lett. **120**, 151301 (2018); T. Braine *et al.* (ADMX Collaboration), Phys. Rev. Lett. **124**, 101303 (2020).
- [15] C. Bartram *et al.* (ADMX Collaboration), Phys. Rev. Lett. **127**, 261803 (2021).
- [16] leidencryogenics.nl.
- [17] B. R. Ko *et al.*, Phys. Rev. D **94**, 111702(R) (2016).
- [18] Michael S. Turner, Phys. Rev. D **42**, 3572 (1990).
- [19] www.attocube.com.
- [20] www.cst.com.
- [21] www.comsol.com.
- [22] T. Yamamoto *et al.*, Appl. Phys. Lett. **93**, 042510 (2008).
- [23] Çağlar Kutlu *et al.*, Supercond. Sci. Technol. **34**, 085013 (2021).
- [24] www.lownoisefactory.com.
- [25] <https://polyphasemicrowave.com>.
- [26] S. Ahn *et al.*, JINST **17**, P05025 (2022).
- [27] S. Lee, J. Phys.: Conf. Ser. **898**, 032035 (2017).
- [28] T. L. Wilson, [arXiv:1111.1183](https://arxiv.org/abs/1111.1183).
- [29] H. Friis, Proc. IRE **32**, 419 (1944).
- [30] A. Savitzky and M. J. E. Golay, Analytical Chemistry, **36**, 1627 (1964).
- [31] R. H. Dicke, Rev. Sci. Instrum. **17**, 268 (1946).
- [32] S. J. Asztalos *et al.*, Phys. Rev. D **64**, 092003 (2001).
- [33] B. M. Brubaker, L. Zhong, S. K. Lamoreaux, K. W. Lehnert, and K. A. van Bibber, Phys. Rev D **96**, 123008 (2017).
- [34] S. Ahn, S. Lee, J. Choi, B. R. Ko, and Y. K. Semertzidis, J. High Energ. Phys. **2021**, 297 (2021).
- [35] Note also that the RBW reduction from 10 to 50 Hz decreases the SNR less than 0.1%.
- [36] J. Jeong, S. Yoon, S. Ahn, J. E. Kim, and Y. K. Semertzidis, Phys. Lett. B **777**, 412 (2018).
- [37] D. Ahn *et al.*, Phys. Rev. Applied **17**, L061005 (2022).